

Three-level Vienna Rectifier with a Brushless and Permanent Magnetless Generator for Wind Energy Conversion Systems

Research paper

Haimanti Bhattacharjee^{1,*}, Debranjana Mukherjee², Chandan Chakraborty¹

¹ Department of Electrical Engineering, Indian Institute of Technology Kharagpur, Kharagpur, India

² Department of Electrical and Computer Engineering, University of Illinois at Urbana-Champaign, Illinois, United States

Received: January 13, 2022; Accepted: April 03, 2022

Abstract: This paper proposes a system design and control technique for a newly developed brushless and permanent magnetless synchronous generator-based variable-speed wind energy generation system, transferring power to a constant voltage dc grid via a three-level Vienna rectifier (VR). The recently established generator named Brushless Induction excited Synchronous Generator (BINSYG) is a wound field synchronous generator (WFSG), whose excitation is developed by controlling an Induction Machine fitted to the same machine structure and sharing the same magnetic core. A new controller is proposed that ensures the stable operation of BINSYG for a wide variation of shaft speeds. VR achieves sinusoidal input current and can control the power factor at its input, which is particularly suitable for wind energy applications. The top and bottom capacitor voltages of the VR are balanced using redundant switching combinations. The system with its proposed control algorithm is modelled in MATLAB/Simulink for a 5 kW rated BINSYG feeding power to a 750 V dc grid. The steady-state and dynamic state simulation results are presented and the controller performance is verified for a wide range of wind speeds. Further, real-time results using the OPAL-RT testbed are presented for the same system to verify the effectiveness of the overall control strategy.

Keywords: brushless and magnetless Synchronous Generator • maximum power point • unity power factor • Vienna Rectifier • Wind Energy Conversion System

1. Introduction

Demand for electrical energy continues to rise rapidly over the decades. To meet this growing energy demand along with the challenging targets set globally for de-carbonisation of climate, there has been an increasing focus on renewable power generation systems (like solar power, wind power, hydropower, tidal power, fuel-cells, etc.). Among these, wind technology has emerged as the fastest developing technology with both onshore and offshore projects coming up. The growth in global wind generation capacity is 53% in the year 2020, with 93 GW of new installations bringing global cumulative wind power capacity to 743 GW. This is due to technical progress in wind turbine operation, improved blade design, favourable wind energy market, policies etc. (Global wind report 2021, 2021). A typical Wind Energy Conversion System (WECS) consists of a wind turbine that converts the wind energy available at its blades to mechanical energy that is driving the shaft of the generator. An electro-mechanical device (Generating system) further converts it to electrical energy. The generated power is fed either to a grid or load. The merits of the dc grid collection system are the absence of reactive power control, absence of frequency control, easy synchronisation of different generators operating in parallel and easy integration into energy storage systems. These factors have led to increased use of dc grid collection systems (Gil et al., 2015).

The main requirements for the wind generator (WG) are higher reliability, minimum maintenance cost and reduced floor area. Taking these constraints into consideration, various generator topologies proposed in the literature are

* Email: haimantibhattacharjee@gmail.com

studied. Doubly Fed induction generator (DFIG) and permanent magnet synchronous generator (PMSG) have developed as widely used generators for wind energy applications. Although DFIGs are advantageous as they require fractional power rated machine side rectifiers (MSRs) connected to their rotor, however, they have some disadvantages such as a narrow speed range of operation ($\approx \pm 30\%$) due to fractional rated power converters and brushes/slip-rings for rotor side connections leading to regular maintenance (Iwański and Łuszczuk, 2017; Prajapat et al., 2020). Brushless DFIGs (BDFIGs) are developed to eliminate the need of brushes and slip-rings (Shipurkar et al., 2017). But these generators have a complex rotor structure thereby increasing design complexity and cost. In contrast, PMSGs have recently gained wide popularity as wind energy generators because of their advantages like higher efficiency and higher power density due to the use of permanent magnets (PMs), absence of brushes/slip-rings and wide speed range of operation (Kumari et al., 2018; Gajewski and Pieńkowski, 2016). However, the availability of PMs for construction is a concern, since their mining is costly and causes environmental pollution. Also, PMSGs require rare-earth materials proportional to the size of the generator, which increases with an increase in generator rating which leads to an increased cost of PMSGs (Pavel et al., 2017). These magnets also suffer from the problem of demagnetisation due to rough handling. Alternatively, wound field synchronous generators (WFSGs) with electrically excited field windings have been investigated for their applicability in WECS (Szulawski and Koczara, 2016). WFSGs are magnet-less with controlled rotor flux that allows a wider speed range of operation. Conventional WFSGs use separate exciter for field excitation, involving brushes/slip-rings. In order to make the excitation system brushless and compact, a power transferring approach through a high frequency rotating exciter is reported (Liu et al., 2016). Though the exciter has become compact, it remains an additional component connected to the same shaft. Hybrid excitation synchronous generators (Patin et al., 2008) have both magnets and field windings on the rotor and in order to combine the advantages of both PMSGs and WFSGs, a WFSG, named Brushless Induction Excited Synchronous Generator (BINSYG) is proposed (Chakraborty and Rao, 2019), where the excitation machine (IM) is housed in the same machine frame, as SG. The two machines (SG and IM) are wound for different pole numbers. The rotor of IM is electrically connected to the field of SG via an uncontrolled rectifier. The voltage induced in the rotor terminals of IM is rectified and is responsible for generating the field voltage of SG. In the proposed approach both power and excitation machines are embedded in the same machine structure. Fixed speed (Chakraborty and Rao, 2019; Bhattacharjee et al., 2020) and limited range of varying speed operation of BINSYG (Rao et al., 2021), with IM operating in power-zero mode have been demonstrated in the literature.

The type of power that is available at the generator terminal is ac. In order to interface the generator to the dc grid, the electrical power output of the generator needs to be converted to dc. There are two categories of WECS, namely, fixed speed and variable speed. Variable speed WGs can operate at maximum power conditions for a range of wind speeds. This is done using a power converter connected to the machine (called as MSRs). The MSR rectifier is controlled such that it converts ac power to dc and feeds maximum electrical power generated by the WG to the dc grid. The power flow in a WECS is unidirectional (i.e. power flows only from the generator to the dc grid). Several ac to dc power converters suitable for MSRs are proposed in the literature (Yamasu et al., 2015). Among these the most commonly used are three-phase two-level pulse width modulated (PWM) rectifiers. The simplest topology is a combination of a diode-bridge rectifier and a dc/dc converter for power control (Rahimi, 2017). The dc/dc converter is used for regulating the power fed to the grid by adjusting the speed of the generator. Although a diode-bridge rectifier is cheap and reliable, it introduces lower-order harmonics in the stator current of the generator that leads to torque oscillations and is unable to control the generator terminal power factor. So bulky LCL filters or additional active rectifiers need to be employed to eliminate these harmonics. The resonance between the LC filter and generator is also an issue that causes poor dynamic performance (Xu and Xie, 2018; Sabrina et al., 2021). These problems can be eliminated using a six-switch three-phase two-level voltage source rectifier (2L VSR). However, a higher number of active switches (six in this case) and their higher voltage rating (voltage stress across each switch in 2L VSR is equal to the dc-link voltage) actually increase the cost and decrease the reliability of the MSR. Efforts have been made to decrease the number of active switches to increase their reliability and provide good power quality of line current by proposing multi-level reduced-switch rectifiers. Several rectifier topologies such as three-level Neutral Point Clamped (3L NPC) rectifiers (Lee and Lee, 2015) and matrix converters (Yang and Zhu, 2010) have been proposed as the MSR. However, increased switch number and complex control limit the use of such converters for WECS. To overcome these limitations, a three-phase three-level (3L) Vienna rectifier (VR) with its characteristics voltage boost capability is a better choice for the MSR because of the following advantages: (i) voltage boost characteristic, (ii) unidirectional power flow through the converter (from source to grid/load),

(iii) controlled power-factor at its input, (iv) ability to have minimum harmonic distortions in the input current, (v) minimum switch requirements (three switches in total) and (vi) absence of a requirement of external hardware for dc-link capacitor voltage balancing. Recently, the use of 3L VR has been demonstrated as the MSR (Luqman et al., 2019; Rajaei et al., 2011; Reddy and Ramasamy, 2018).

In terms of control strategies, the simplest control strategy for VR is hysteresis-based control. The terminal voltages of the grid are sensed, and a rotating vector whose magnitude is unity is generated. This is multiplied by the dc current magnitude generated from the PI voltage-controller that regulates the output dc voltage. Three-phase rotating current (reference waveform) is generated and fed to the hysteresis controller, along with the three-phase sensed currents (Maswood et al., 2011). However, this method depends on sensing the terminal voltage of the grid/generator, which decreases the reliability of the system. Moreover, if the terminal voltage is not sinusoidal (as in the case of a synchronous generator connected to a rectifier), this control strategy will introduce harmonics in the stator current of SG that will affect the power quality. One-cycle control strategy for VR control is proposed (Minibock and Kolar, 2005), where the sensed current along with the zero-sequence current generates the modulation signals for the VR, without the use of any voltage sensors. However, the controller design is quite complex and improper design leads to poor power quality of the system. Several other control strategies such as the double-loop control strategy (Mukherjee and Kस्था, 2015), predictive control of VR (Lee and Lee, 2017) and sliding mode current control (Flores-Bahamonde et al., 2014) are proposed in the literature.

This article presents the performance of a variable speed wind turbine driving a generator, BINSYG, when feeding power to a stiff dc grid. A three-switch VR is used to interface BINSYG to the dc grid. A control algorithm is proposed to transfer maximum power generated by BINSYG to the dc grid for any wind speed while developing the required excitation for SG by IM stator current control via a two-level (2L) voltage source inverter (VSI). The stator current of SG is controlled such that it is maintained at unity power factor (upf) with the stator terminal voltage of SG, without using ac voltage sensors. The harmonics of stator current of SG are also minimised using proper switching combinations generated using double closed-loop vector control of VR. Simulation results obtained from MATLAB/Simulink and real-time results using OPAL-RT testbed under steady-state and transient state wind speed commands confirm the effectiveness of the proposed control strategy on the power network.

This article is arranged as follows. The modelling of the proposed power network, where BINSYG is connected to the dc grid via VR, and is driven by a wind turbine is analysed in Section 2. The overall control structure is presented in Section 3. The working of the controller is checked under steady-state and transient conditions in Section 4 using MATLAB/Simulink simulation results. These are again confirmed by presenting real-time results using the OPAL-RT testbed in Section 5. Finally, conclusions are drawn in Section 6.

2. Analysis and Modelling of BINSYG Wind Turbine for Connection to DC grid via 3L VR

This section proposes the power network system for wind energy conversion. It consists of four parts: (i) the wind turbine, (ii) the generator BINSYG, (iii) the 2L VSI that acts as excitation controller for SG and (iv) the 3L VR that is required for ac/dc power conversion and control of power flow to dc grid. The basic system configuration for the proposed variable speed wind turbine connected BINSYG feeding power to the dc grid is shown in Figure 1. The WT

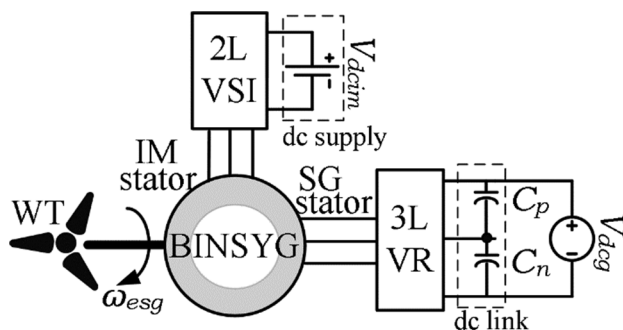


Fig. 1. System configuration for variable speed wind turbine connected BINSYG feeding power to DC grid. BINSYG, brushless induction excited synchronous generator; VR, Vienna rectifier; VSI, voltage source inverter.

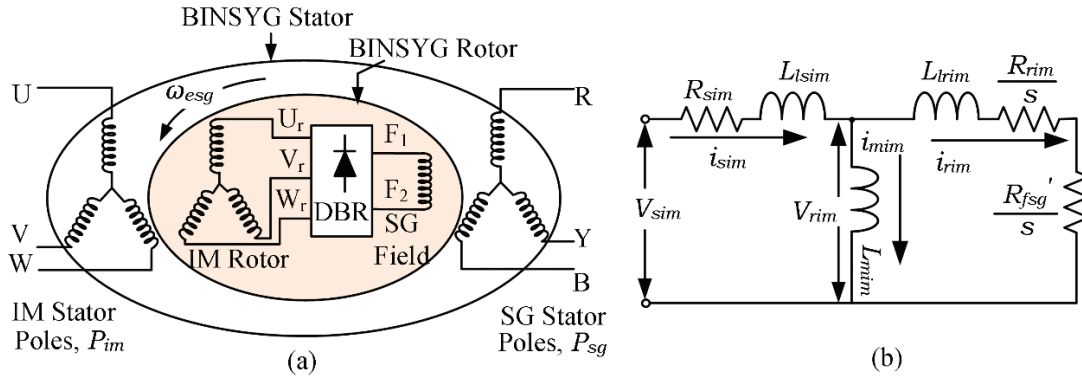


Fig. 2. Brushless and Permanent Magnet less BINSYG. (a) Structural layout and (b) Winding configuration. BINSYG, brushless induction excited synchronous generator; DBR, diode bridge rectifier.

blades are rotated by the wind which in turn rotates the shaft of the generator. The mechanical power of the shaft is converted to electrical power by BINSYG, according to the speed of the wind blowing. In this proposed system, BINSYG is a recently developed SG with electrical excitation, with an in-built three-phase IM sharing the same magnetic core, for the development and control of excitation requirements of SG (Chakraborty and Rao, 2019). The structural layout and available terminals of the generator are shown in Figure 2(a). The two machines (SG and IM) are magnetically decoupled since their pole numbers are different. This prevents induction of voltage in one set of winding of SG due to the current flowing through in the other windings of IM (and vice versa). The field winding of SG is connected to the rotor winding of IM via a rotating diode bridge rectifier (DBR), hence modifying the rotor circuit as shown in Figure 2(b). Consequently, the voltage induced in the rotor of IM can be supplied to the field winding of SG after rectification. This arrangement makes BINSYG brushless and free from PMs. The generator BINSYG considered here is designed with SG wound for 4 Poles and IM for 6 Poles, so this particular generator is named as 4/6 BINSYG. Due to their decoupled nature, the generator behaves as an SG and IM connected on the same shaft. A 3-phase 2L VSI is connected to the stator terminals of IM. The VSI is responsible for controlling the magnitude and frequency of stator current of IM, required for generating the appropriate field excitation for SG. The control algorithm for VSI decides the operating mode of IM (generating mode, motoring mode or plugging mode), depending upon the application targeted by BINSYG. It is the feeding power to a stiff dc grid. The ac power generated by BINSYG is converted to dc and transferred to the dc grid by a 3L VR connected to the stator terminals of SG. No interfacing inductors or passive filters inductor-capacitor filter/inductor-capacitor-inductor filter (LC/LCL) are used to connect BINSYG to the VR, since the leakage inductance of the generator is enough to keep the current ripple low. VR ensures sinusoidal stator current of the generator, hence reducing copper losses and heating in SG stator windings. It also allows the generator terminal power factor (pf) to be controlled at unity for maximum power per ampere operation of BINSYG. The dc grid is a stiff grid with voltage maintained constant at 750 V. The proposed system is modelled and analysed in the upcoming section.

2.1. Wind turbine modelling

The wind-turbine mechanical power P_{wt} for any wind speed v_w is expressed as follows (Heier, 2014):

$$P_{wt} = \frac{\rho_{air} \pi R^2 C_p(\lambda, \beta) v_w^3}{2} \quad (1)$$

where ρ_{air} is the density of air ($\rho_{air} = 1.205 \text{ kg/m}^3$), R is the wind-turbine radius, $C_p(\lambda, \beta)$ is the power coefficient, β is the pitch-angle and λ is the tip speed ratio (TSR). Therefore, from Eq. (1), we find that for a particular turbine-blade parameter, the maximum wind power generated $P_{wt(max)}$ is related to the shaft speed N as follows:

$$P_{wt(max)} = \frac{\rho_{air} \pi R^5 C_p(max) \alpha^3 \left(\frac{2\pi}{60}\right)^3}{2 \lambda_{opt}^3} N^3 \quad (2)$$

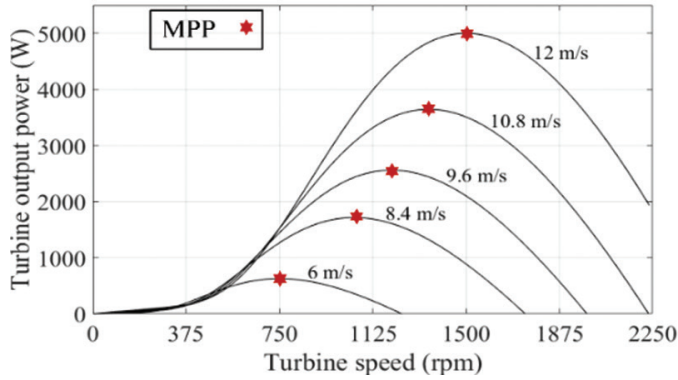


Fig. 3. Wind-turbine power versus shaft speed for different wind speeds. MPP, maximum power point.

Table 1. Wind turbine parameters

Wind turbine parameter	Value
Rated power (P_{wt})	5,000 W
Rated shaft speed (N)	1,500 rpm
Rated wind speed (v_w)	12 m/s
Rotor radius (R)	1.785 m
Gear ratio (α)	0.3466
Optimum TSR (λ_{opt})	8.1
Maximum power coefficient ($C_{p(max)}$)	0.48

TSR, tip speed ratio; rpm, revolutions per minute.

where $C_{p(max)}$ is the maximum value of $C_p(\lambda, \beta)$ with $\lambda = \lambda_{opt}$ and $\beta = 0$, a is the gear-ratio and λ_{opt} is the optimum TSR. The torque of the wind turbine T_{wt} is obtained as

$$T_{wt} = \frac{P_{wt}}{(2\pi/60)N} \quad (3)$$

The power captured by the wind turbine versus shaft speed, for different wind speeds obtained from Eq. (2) is plotted in Figure 3 and the wind-turbine parameters are mentioned in Table 1. The maximum power that can be captured by the turbine blades for each wind speed and turbine speed is marked on the plot. The pitch angle of the wind turbine, β , is constant ($\beta = 0$). The cut-in and rated wind speeds are 6 m/s and 12 m/s, respectively. If the wind speed is between 6 m/s and 12 m/s, the turbine power and torque are generated as per Eqs. (1–3).

2.2. BINSYG modelling

The overall torque dynamics of BINSYG as a function of rotor mechanical angular speed (ω_{msg}) is

$$T_{esg} \pm T_{eim} = J \frac{d\omega_{msg}}{dt} + B\omega_{msg} + T_{load} \quad (4)$$

where T_{esg} is the torque developed by SG, T_{eim} is the torque developed by IM, T_{load} is the load torque, J is the moment of inertia and B is the damping coefficient. In Eqn. (4), the '+' sign is used for IM is operating in motoring mode and '-' sign is used when operating in generating or plugging mode. The parameters of BINSYG are obtained using open circuit and short circuit tests and are tabulated in Table 2. The rotor of IM is electrically connected to the field circuit of SG via a DBR, and as a result, the effective rotor resistance of IM (R_{reffim}) is modified as shown in Figure 2(b). The modified resistance (R_{reffim}) is the sum of field resistance of SG reflected on the IM stator side (R_{tsg}) that can

Table 2. BINSYG parameters

SG parameter	Value	IM parameter	Value
Rated power ($P_{\text{esg}(\text{rated})}$)	5,000 W	Rated power	1,100 W
Rated terminal voltage (L-L)	415 V	Rated terminal voltage (L-L)	110 V
Rated speed (N_{rated})	1,500 rpm		
Pole number (P_{sg})	4	Pole number (P_{im})	6
Stator resistance (R_{sg})	1.32 Ω	Stator resistance (R_{sim})	2.4 Ω
Field resistance (R_{fsg})	40.8 Ω	Rotor resistance (R_{rim})	2.93 Ω
Field inductance (L_{fsg})	2 H	Modified rotor resistance (R_{reffim})	17.5 Ω
Synchronous inductance (L_{sg})	110.5 mH	Stator and rotor inductance ($L_{\text{sim}} = L_{\text{rim}}$)	48.375 mH
Leakage inductance (L_{lsq})	3.5 mH	Magnetising inductance (L_{rim})	45.5 mH
Turns ratio ($N_{\text{fsg}}/N_{\text{sg}}$)	8.047	Turns ratio ($N_{\text{sim}}/N_{\text{im}}$)	0.845

BINSYG, brushless induction excited synchronous generator.

be calculated by balancing of active power on both sides of DBR and rotor resistance of IM (R_{rim}). As a result, the time-constant of the rotor of IM (τ_{rim}) is also modified (Bhattacharjee et al., 2021).

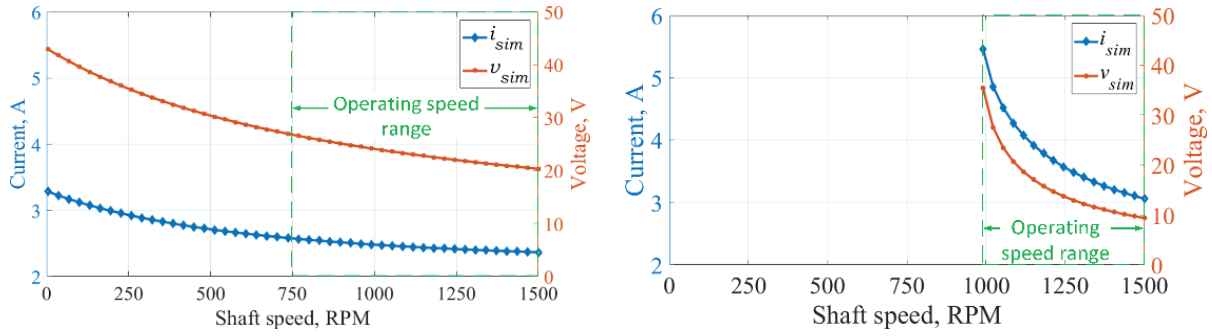
SG is desired to be operated in fixed E/f mode, i.e. the induced voltage of SG is directly proportional to the frequency/speed of the shaft. As a result, the field current of SG (i_{fsg}) remains constant. The objective of IM in BINSYG is to develop the required excitation current for SG. IM can develop this current by operating in any of the three different modes, namely plugging mode, generating mode and motoring mode. The IM can be made to function in any of these modes by adjusting the frequency of its stator current, which is done by a two-level (2L) VSI. When the stator frequency of IM (ω_{sim}) is greater than its rotor frequency (ω_{eim}), the IM is said to be operating in motoring mode while the IM is said to be operating in generating mode when the value of ω_{sim} is less than ω_{eim} . When ω_{sim} is negative, the operation of IM is shifted to plugging mode. In literature, BINSYG has been operated in standalone mode with the IM operating in a power-zero operating point (Chakraborty and Rao, 2019; Bhattacharjee et al., 2020). The advantage of this operating point is that the IM draws no active power from the supply connected to its stator. However, there are certain limitations of this operating point such as (i) stable speed range of operation of BINSYG is limited (1,000 rpm to 1,500 rpm) when IM is operated in power-zero point and (ii) dc power supply is required for pre-charging the dc-link capacitor connected to 2L VSI at starting. Therefore to operate BINSYG in a wider speed range the operating point of IM must be shifted from the power-zero point. So a new control strategy is proposed for the control of IM via 2L VSI, in which IM is operated in plugging mode by operating at a constant stator frequency (ω_{sim}) of -314 rad/s, so that BINSYG can be controlled under stable conditions even when shaft speed is below 1,000 rpm. The stator current and voltage of IM while in plugging mode, as a function of BINSYG shaft speed is obtained as,

$$i_{\text{fsg}} = 2.1 \text{ A}, \quad i_{\text{rim}} = \left(\frac{1}{N_{\text{sim}}/N_{\text{rim}}} \sqrt{\frac{2}{3}} i_{\text{fsg}} \right) \quad (5)$$

$$i_{\text{sim}} = \frac{\left(\frac{R_{\text{reff}}}{s} + j\omega_{\text{sim}}L_{\text{trim}} \right)}{j\omega_{\text{sim}}L_{\text{mim}}} \left(\frac{1}{N_{\text{sim}}/N_{\text{rim}}} \sqrt{\frac{2}{3}} i_{\text{fsg}} \right) \quad (6)$$

$$v_{\text{sim}} = i_{\text{sim}} (R_{\text{sim}} + j\omega_{\text{sim}}L_{\text{sim}}) + i_{\text{rim}} \left(\frac{R_{\text{reff}}}{s} + j\omega_{\text{sim}}L_{\text{trim}} \right) \quad (7)$$

With variation in shaft speed, the slip s vary and the nature of stator current and voltage of IM are displayed in Figure 4. The advantages of the proposed mode of control are highlighted by comparing the nature of stator current and voltage of IM obtained in the case of plugging mode [shown in Figure 4(a)] to that obtained in the case of power-zero mode [shown in Figure 4(b)]. The cut-in speed of the wind turbine is 6 m/s, and hence the wind turbine can drive the generator BINSYG while letting it to operate at maximum power point (MPP) conditions from 750 rpm



(a) (b)
Fig. 4. Stator current and voltage of IM while operating in (a) plugging mode and (b) power-zero mode.

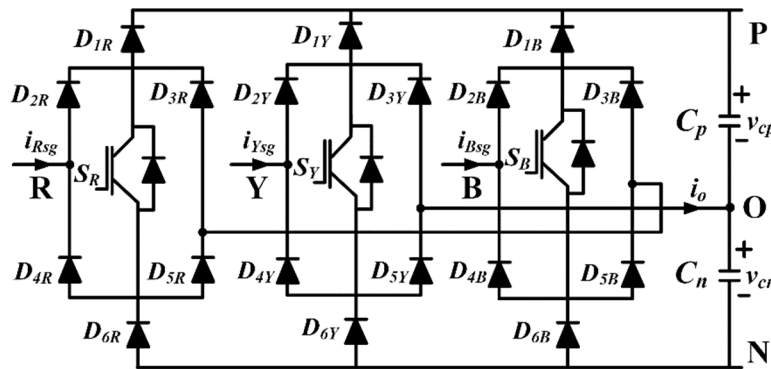


Fig. 5. Power circuit for 3-phase 3L VR. VR, Vienna rectifier.

to 1,500 rpm. When IM is operated in plugging mode, the plot in Figure 4(a) shows that over the entire shaft speed range (750 rpm to 1,500 rpm) the values of stator current (i_{sim}) and voltage (v_{sim}) of IM are at below their rated values. However operating in power-zero mode limits the generator speed to 1,000 rpm, because the operation of IM is unstable when the shaft speed falls below 1,000 rpm (Rao et al., 2021). Hence the stable operating speed range of BINSYG, in this case, ranges only from 1,000 rpm to 1,500 rpm, as marked in Figure 4(b). Consequently, the proposed control strategy where IM is operated in plugging mode allows wide speed range operation of BINSYG without IM losing its stability.

2.3. VR

The PWM rectifier that is used to extract power from the variable speed BINSYG, is a 3-phase 3L unidirectional pf corrector rectifier, also known as VR. The input (ac terminals) of VR is connected to the stator terminals of SG. VR has the capability to boost voltage at its output and comprises of one active switch per phase, i.e. a total of three active switches, as shown in Figure 5. There are six diodes (D_{1R} to D_{6R}) per phase. The dc bus is split into two parts and two capacitors are connected in series, with 'O' as its mid-point. The power is fed to the dc grid by connecting the output/dc terminals to a constant voltage dc grid (voltage, V_{dcg}). Under steady-state, the top and bottom capacitor voltages (v_{cp} and v_{cn}) are balanced at half the dc grid voltage ($V_{dcg}/2$) by generating appropriate switching combinations. Several advantages of VR are: (i) minimum number of active switches (ii) reduced blocking voltage of the switches and the diodes leading to reduced switching loss and (iii) improved power quality of line currents. The pole voltage of VR (v_{xO}) depends not only on the switching status of switch S_{x_i} , but also on the direction of phase currents (i_{Xsg}) passing through the input terminal of that phase which is obtained as

$$v_{xO} = \frac{V_{dcg}}{2} (1 - S_X) \text{sgn}(i_{Xsg}) \quad (8)$$

Table 3. Switching states and respective voltage/current w.r.t midpoint (O) (when $i_{Rsg} > 0, i_{Ysg} < 0, i_{Bsg} < 0$)

S_R	S_Y	S_B	V_{RO}	V_{YO}	V_{BO}	i_o
0	0	0	$V_{dcg}/2$	$-V_{dcg}/2$	$-V_{dcg}/2$	0
0	0	1	$V_{dcg}/2$	$-V_{dcg}/2$	0	i_{Bsg}
0	1	0	$V_{dcg}/2$	0	$-V_{dcg}/2$	i_{Ysg}
0	1	1	$V_{dcg}/2$	0	0	$-i_{Rsg}$
1	0	0	0	$-V_{dcg}/2$	$-V_{dcg}/2$	i_{Rsg}
1	0	1	0	$-V_{dcg}/2$	0	$-i_{Ysg}$
1	1	0	0	0	2	$-i_{Bsg}$
1	1	1	0	0	0	0

VR, Vienna rectifier.

where X is the phase $R; Y; B$, $sgn(i_{Xsg})$ is +1 (when $i_{Xsg} > 0$) and -1 (when $i_{Xsg} < 0$), S_x is the switch status (i.e. when the switch is ON, $S_x = 1$ and $S_x = 0$ when OFF). The pole voltages for a particular direction of phase current and eight different switching combinations are obtained using Eqn. (8) and tabulated in Table 3.

3. Overall Control Structure for BINSYG Connected to DC Grid via 3L VR

For a fixed speed or limited varying speed operation of BINSYG (where shaft speed varies from 1,000 rpm to 1,500 rpm), power-zero controllers can be implemented (Rao et al., 2021). However, for speeds below 1,000 rpm, the power-zero controller makes the operation of IM unstable, and hence BINSYG loses its stability. Therefore, for BINSYG to operate at low speeds (below 1,000 rpm) a new controller for IM needs to be developed. So a new controller is proposed in which IM is operated in plugging mode to enable a wider speed range of operation of BINSYG. The overall control strategy can be broadly divided into two sections: (i) control of 2L VSI connected to stator of IM and (ii) control of 3L VR connected to stator of SG. The motivation for control of 2L VSI is to develop a rated field current for the stable operation of BINSYG when wind speed is varying. The purpose of control of 3L VR is to command the power flow to the dc grid and regulate the pf at the stator terminal of SG.

3.1. Control of 2L VSI connected to stator of IM

A new controller for 2L VSI connected to IM that allows BINSYG to operate at maximum power conditions for a wide range of wind speeds is illustrated in the following section. IM is operated in plugging mode with constant stator frequency (ω_{sim}) to generate reference d axis component of stator current (i_{dsim}^*). Constant E/f operation of SG requires the field current (i_{fsg}) to remain constant at its rated value. The rotor voltage equations of IM with modified rotor circuit, when aligned to rotor-flux oriented reference (such that, $\psi_{qrim} = 0$) frame makes reference q- axis component of stator current (i_{qsim}^*) directly proportional to field current (i_{fsg}). The reference value of i_{qsim}^* is calculated for the development of the rated field current. In rotor-flux oriented indirect vector control of IM, the slip speed (ω_{slim}) required for the orientation can be calculated using Eqn. (9), where the actual d and q axis components of stator current (i_{dsim}, i_{qsim}) are sensed (Moallem et al., 2001; Bose, 2002),

$$\omega_{slim} = \frac{i_{qsim}}{\tau_{rim} i_{dsim}} \quad (9)$$

here, $\tau_{rim} = (L_{rim}/R_{r_{eff_im}})$ is the time constant of the modified rotor circuit of IM. The shaft speed of BINSYG (ω_{esg}) is sensed (in elec rad/s) and the corresponding rotor frequency of IM ω_{eim} is,

$$\omega_{eim} = \frac{P_{im}}{P_{sg}} \omega_{esg} \quad (10)$$

where P_{im} and P_{sg} are the pole number for IM and SG, respectively ($P_{im} = 6$, $P_{sg} = 4$). The stator frequency of IM (ω_{sim}) is calculated from Eqns. (9) and (10), and the related equation is

$$\omega_{sim} = \omega_{sl} + \omega_{eim} \quad (11)$$

The rotor position ρ required for rotor flux orientation is obtained from Eqn. (11) as,

$$\rho = \int \omega_{sim} dt \quad (12)$$

The reference values, i_{dsim}^* (from the control of stator frequency) and i_{qsim}^* (from rotor flux orientation along the d-axis) are calculated as per the following equations:

$$i_{dsim}^* = \left(k_{pd} + \frac{k_{id}}{s} \right) (\omega_{sim}^* - \omega_{sim}) \quad (13)$$

$$i_{qsim}^* = -\frac{L_{rim}}{L_{mim}} \left(\frac{\sqrt{2}}{(N_{sim}/N_{rim})} \sqrt{\frac{2}{3}} i_{fsg} \right) \quad (14)$$

where k_{pd} and k_{id} are the PI controller parameters (values mentioned in Table 4) used for d axis current control of IM. The actual and reference d and q axis components of stator current of IM (i_{dsim} and i_{qsim} , i_{dsim}^* and i_{qsim}^*) are fed to the hysteresis current controller to generate the modulation signals for 2L VSI.

3.2. Control of 3L VR connected to stator of SG

The generated power is transferred to the dc grid and controlled using q axis component of the stator current of SG (or, the input current of VR). SG is operated such that maximum power is extracted from the wind. This is achieved using maximum power point tracking (MPPT) scheme that generates the reference q axis component of stator current of SG (i_{qsg}^*) such as

$$i_{qsg}^* = \frac{P_{wt}(rated)}{e_{sg}} \frac{N(rated)^3}{N^3} \quad (15)$$

The input pf of VR is controlled using d axis component of stator current of SG (i_{dsg}) such that

$$\frac{i_{dsg}}{v_{dsg}} = \frac{i_{qsg}}{v_{qsg}} \quad (16)$$

The d and q axis components of the terminal voltage of SG (v_{qsg}^* , v_{dsg}^*) are obtained as

$$v_{qsg}^* = -R_{sg} i_{qsg} - L_{sg} \frac{d i_{qsg}}{dt} - \omega_{esg} L_{sg} i_{dsg} + e_{sg} \quad (17)$$

$$v_{dsg}^* = -R_{sg} i_{dsg} - L_{sg} \frac{d i_{dsg}}{dt} + \omega_{esg} L_{sg} i_{qsg} \quad (18)$$

where e_{sg} is the induced voltage of SG, R_{sg} is the stator resistance of SG and L_{sg} is the synchronous inductance of SG. Consequently, putting Eqns. (17) and (18) in Eqn. (16), and considering steady-state conditions, the quadratic equation for deriving the reference d axis component of stator current of SG (i_{dsg}^*) is

$$\begin{aligned} \omega_{esg} L_{sg} i_{dsg}^{*2} - e_{sg} i_{dsg}^* + \omega_{esg} L_{sg} i_{qsg}^{*2} &= 0 \\ \Rightarrow i_{dsg}^{*2} - \frac{e_{sg}}{\omega_{esg} L_{sg}} i_{dsg}^* + i_{qsg}^{*2} &= 0 \end{aligned} \quad (19)$$

Solving Eqn. (19), the value of i_{dssg}^* is given by

$$i_{dssg}^* = \frac{e_{sg}}{2\omega_{esg}L_{ssg}} \pm \sqrt{\left(\frac{e_{sg}}{2\omega_{esg}L_{ssg}}\right)^2 - (i_{qssg}^*)^2} \quad (20)$$

Since i_{fsq} is proportional to i_{qsim}^* , the value of e_{sg} is estimated from the sensed shaft speed (ω_{esg}) is as follows:

$$e_{sg} = k_e \omega_{esg} |i_{qsim}^*| \quad (21)$$

The position of the voltage vector (θ_{sg}) is sensed from the position sensor and the corresponding cosine and sine components of this rotor position angle are obtained for voltage vector orientation. Two current sensors are used to sense the stator currents of SG (i_{Rsg} , i_{Ysg}) and are oriented according to the rotor position angle θ_{sg} . PI controllers used for current control on the SG-side generate the reference d and q axis components of the terminal voltage of SG (v_{qssg}^* , v_{dssg}^*) as per Eqns. (17) and (18). Feed-forward term (e_{sg}) is computed using Eqn. (21) and added for decoupled control. The bandwidth of the PI controller is 1,000 Hz, and the PI parameters are calculated accordingly. Conversion from dq to abc reference frame is done and modulation index of the VR, m is determined using

$$m = \frac{v_{phsg}(1)}{0.5V_{dcg}} \quad (22)$$

where $v_{phsg}(1)$ is the fundamental component of the PWM phase terminal voltage of SG. The modulation index value is thus varied according to the varying wind speed. The switching pulses of 3L VR are generated by Phase-shifted Pulse Width Modulation (PSPWM) technique. To obtain the desired number of levels in the output voltage of the converter, the dc-link capacitor voltages need to be balanced. The capacitor voltage of the bottom dc-link capacitor (v_{cn}) is sensed and subtracted from the reference value ($V_{dcg}/2$). A simple dc voltage balancing controller involving the use of a PI controller is used to generate the redundant switching pulses required for capacitor charge and discharge balancing. The overall control structure is shown in Figure 6.

4. Simulation Results

The proposed power network topology consisting of the generator BINSYG, the controlled converters: 3L VR for control of SG and 2L VSI for control of IM, together with its overall control strategy is modelled in MATLAB/Simulink environment. The performance of the overall system with its controllers is investigated for steady and varying wind speeds. The wind turbine parameters are obtained from Table 1, while the BINSYG parameters are obtained from Table 2 and other power networks and controller parameters are obtained from Table 4. The simulation results displayed in Figures 7 and 8 show the performance of the system under steady-state and step changes in wind speed.

4.1. Steady-state results

Steady-state simulations are performed using MATLAB/Simulink for two different steady wind speeds and the results are presented in Figure 7. The results obtained for the two different cases are compared to study the performance of the system. Figure 7((a), (d)) shows the line voltage (RY-line) for steady wind speeds v_w of 7.2 m/s and 12 m/s. With the increase in wind speed, the modulation index of the rectifier, m increases and the rms value of the line voltage of SG increases. Figure 7((b), (f)) shows the phase (R-phase) voltage of SG terminal (both the PWM voltage, v_{RN} and its fundamental component ($v_{RN(1)}$, calculated using Eqn. (21)) along with the R-phase stator current of SG (i_{Rsg}). The current plot is multiplied by a gain of 20, to clearly study the waveform. The plot shows that under both the cases, the stator current and phase voltage of SG are in phase. This allows the SG to operate at unity pf so that it can transfer maximum active power to the dc grid. The

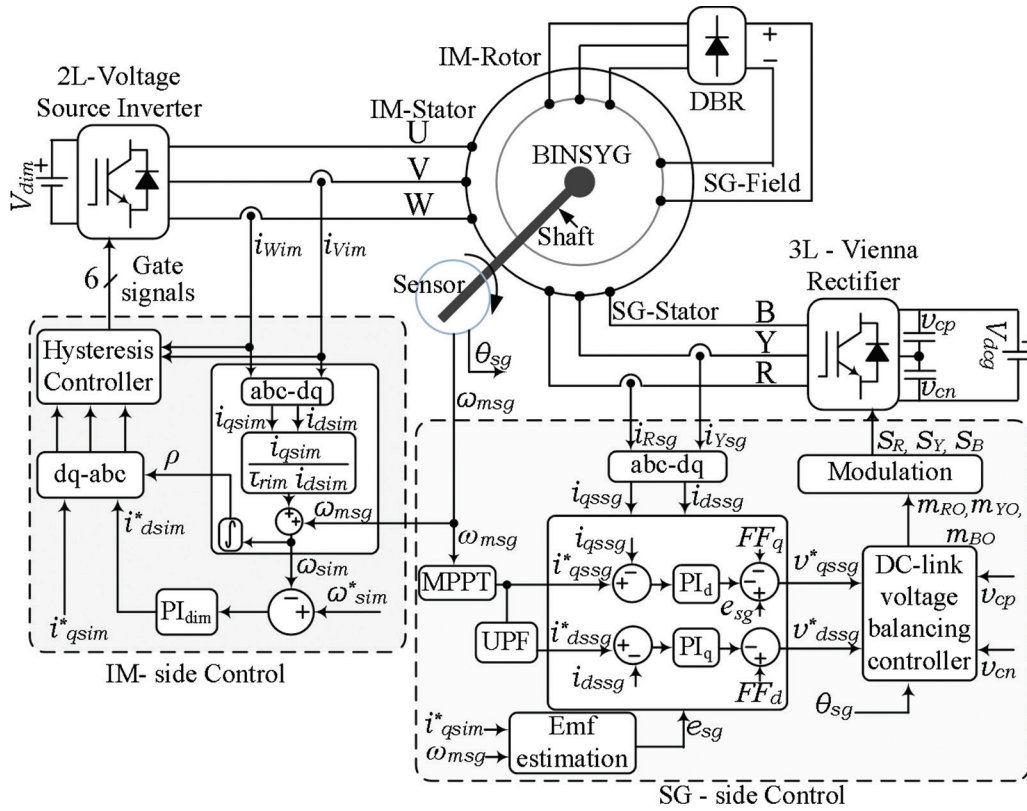


Fig. 6. Proposed overall control strategy for the dc microgrid system. BINSYG, brushless induction excited synchronous generator; DBR, diode bridge rectifier.

Table 4. System and controller parameters

Parameter	Value
DC Grid voltage (V_{dcg})	750 V
DC supply voltage to 2L VSI (V_{dcim})	150 V
DC link top and bottom capacitor (C_p and C_n)	3,000 μ F
IM-d-axis PI controller parameters (k_{pidim} and k_{idim})	0.002, 2
SG-d-axis PI controller parameters (k_{pid} and k_{id})	22, 8,293.88
SG-d-axis PI controller bandwidth (ω_{cdd})	1,000 Hz
SG-q-axis PI controller parameters (k_{pid} and k_{iq})	22, 8,293.88
SG-q-axis PI controller bandwidth (ω_{cqd})	1,000 Hz
VR dc-link voltage balancing PI controllers (k_{pid} and k_{iq})	0.25, 2.5
Switching frequency of VR (f_{sw})	4,000 Hz

VR, Vienna rectifier; VSI, voltage source inverter.

induced voltage of SG is maintained such that it is proportional to the shaft speed of BINSYG. As a result, with an increase in wind speed, the number of levels in the phase voltage increases with an increase in wind speed and the fundamental component of phase voltage of SG increases as demonstrated in the plot. Figure 7((c), (g)) shows the three-phase stator current of SG (i_{ssg}) under the condition of the two wind speeds. With an increase in wind speed, the MPPT algorithms adjust the rotational speed of BINSYG which is done by increasing the current reference of the SG stator current. Therefore with the increase in wind speed, the rms value of stator current of SG increases.

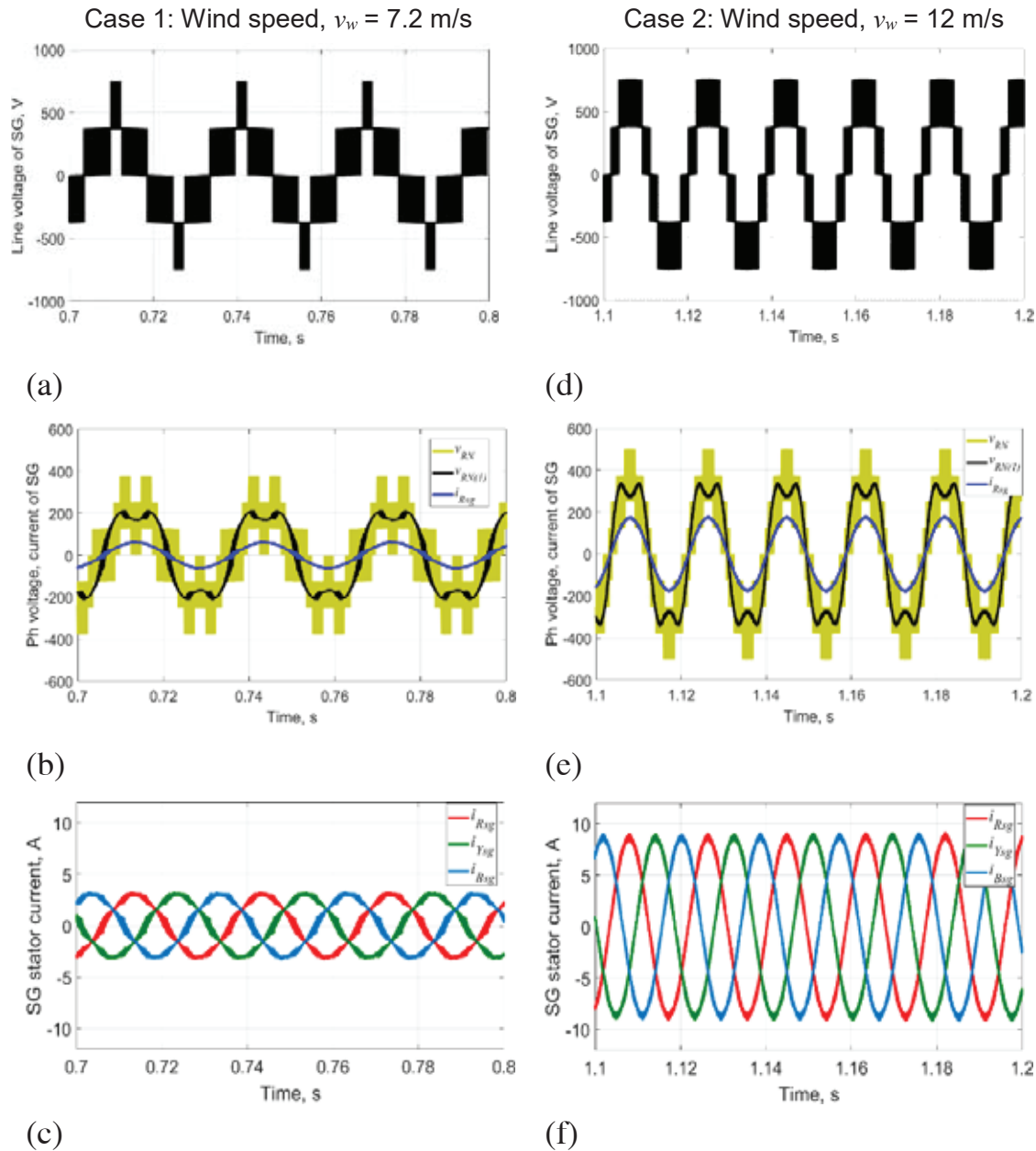


Fig. 7. Steady-state performance of wind turbine connected BINSYG. Case1: when the steady wind speed, v_w is 7.2 m/s. (a) RY-Line voltage of SG (V_{RY}), (b) R-Phase Voltage (PWM and fundamental) and R-phase stator current of SG (V_{RN} , $V_{RN(1)}$, i_{Rsg}) and (c) three-phase stator current of SG (i_{sg}). Case2: when the steady wind speed, v_w is 12 m/s. (d) RY Line voltage of SG (V_{RY}), (e) R-Phase Voltage (PWM and fundamental) and R-phase stator current of SG (V_{RN} , $V_{RN(1)}$, i_{Rsg}) and (f) three-phase stator current of SG (i_{sg}). BINSYG, brushless induction excited synchronous generator; PWM, pulse width modulated.

4.2. Transient results

Transient state simulation results are performed to check the dynamic behaviour of the proposed control on the power network when the system experiences a disturbance in wind speed, and the results are presented in Figure 8. The disturbance is considered as a step-change in wind speed v_w from 7.2 m/s to 12 m/s at time, $t = 1.0$ s and from 12 m/s to 7.2 m/s at time, $t = 1.8$ s. The wind speed dynamics considered are displayed in Figure 8(a). According to the change in wind speed, the wind turbine's torque and power change. The wind turbine is driving the shaft

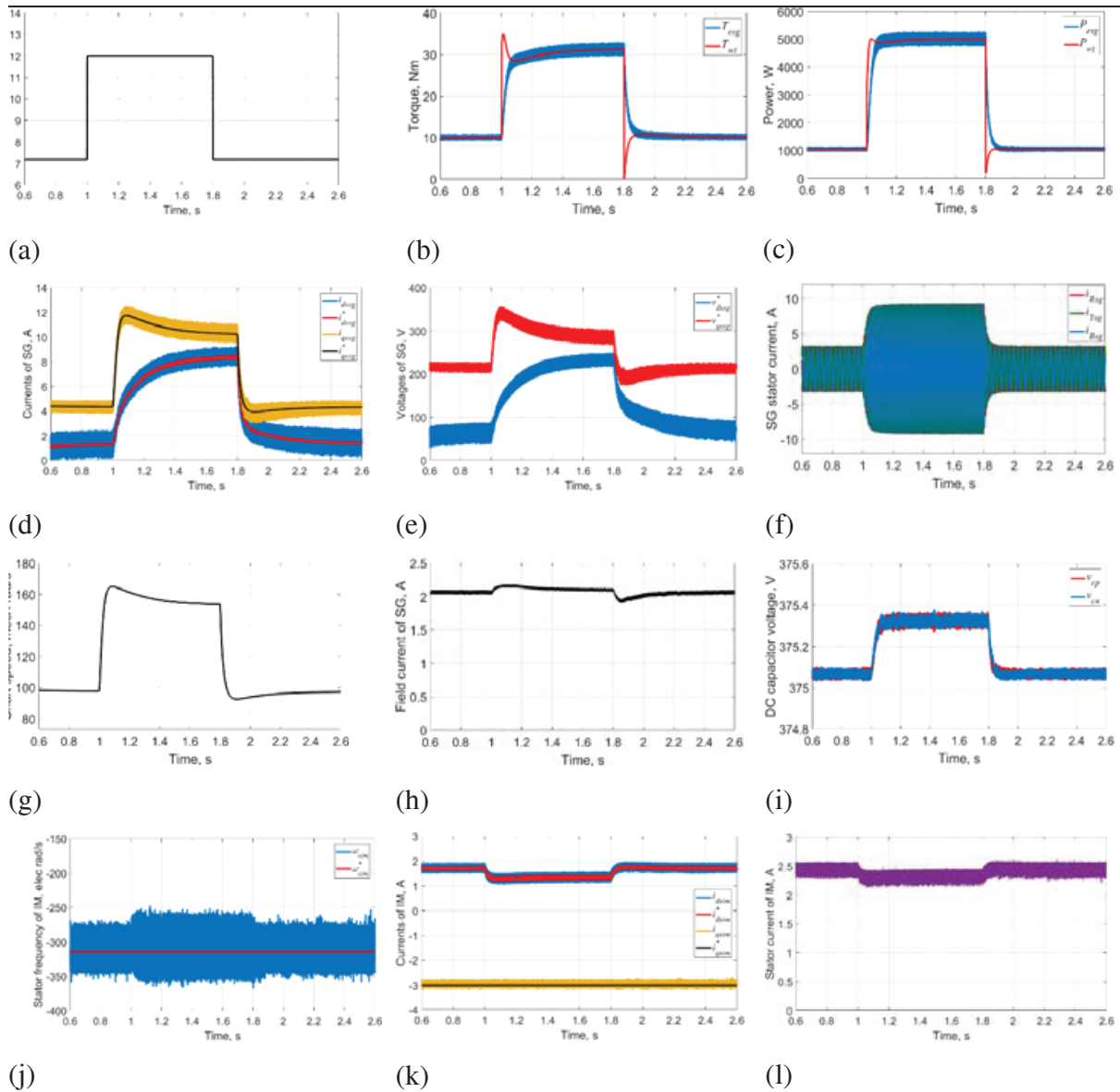


Fig. 8. Transient state performance of wind turbine connected BINSYG. (a) variation in wind speed, (b) wind turbine torque and torque developed by SG, (c) wind turbine power and electrical power generated by SG, (d) reference and actual d and q axis components of stator current of SG, (e) d and q axis components of stator voltage of SG, (f) three-phase stator current of SG, (g) shaft speed of BINSYG, (h) field current of SG, (i) top and bottom capacitor voltages of dc bus, (j) reference and actual stator frequency of IM, (k) reference and actual d axis and q axis stator current of IM and (l) rms value of stator current of IM. BINSYG, brushless induction excited synchronous generator.

of BINSYG. The mechanical torque of the wind turbine (T_{wt}) is equal to the torque developed by SG (T_{esg}), and is proportional to the square of the shaft speed, N . This is shown in Figure 8(b). The maximum mechanical power developed by the wind turbine is proportional to the cube of the shaft speed (obtained in Eqn. (2)). The mechanical power developed by the wind turbine (P_{wt}) and the electrical power generated by the SG (P_{esg}) are shown in Figure 8(c). The power changes from 1,080 W (when $v_w = 7.2$ m/s) to 5,000 W (when $v_w = 12$ m/s) and back to 1,080 W (when $v_w = 7.2$ m/s). The electrical power generated by SG is controlled by the MPPT control strategy, which is done by adjusting the reference q axis component of the stator current of SG (i_{qssg}^*). The pf at the input of VR (SG stator terminal) is adjusted to unity by tuning the reference d axis component of stator current of SG (i_{dssg}^*). The actual d and q axis components of stator current of SG (i_{dssg} , i_{qssg}) are sensed. The reference and actual current

components are shown in Figure 8(d). The actual current follows the reference value and this is done by the VR-side current controller that consists of a PI controller. The VR current controller generates the reference d and q axis terminal voltage components of SG (v_{dssg}^* , v_{qssg}^*), as shown in Figure 8(e). Figure 8(f) shows the three-phase stator current of SG (i_{ssg}). It is clear from the plot that the rms value of SG stator current increases with an increase in wind speed to maintain MPP operation. The shaft angular speed changes from 94.2 mech rad/s (or 900 rpm) at $v_w = 7.2$ m/s to 157 mech rad/s (or 1,500 rpm) at $v_w = 12$ m/s and back to 94.2 mech rad/s (or 900 rpm) at $v_w = 7.2$ m/s. The shaft speed of BINSYG is sensed and the variation during a step change in wind speed is shown in Figure 8(g). It can be inferred from the figure that the IM-side controller is capable of driving BINSYG at shaft speeds lower than 1,000 rpm. The field current of SG developed by IM current control is plotted in Figure 8(h). The field current almost remains constant at a rated value of 2.1 A, throughout because of constant E/f control of SG. The top and bottom dc bus capacitors (C_p , C_n) are balanced at one-half the dc grid voltage ($V_{dcg}/2$) by injecting proper zero sequence current, as shown in Figure 8(i). The IM stator current control is used for developing the field current of SG. IM is operated in plugging mode using the d axis current control that is done by regulating the stator frequency of IM to a constant reference value, ω_{sim}^* of -314 elec rad/s. The actual stator currents of IM are sensed and converted to d and q components and the slip speed is calculated from Eqn. (9). The stator frequency of IM is calculated using Eqn. (10) and (11). The reference and actual stator frequency of IM are plotted in Figure 8(j). It shows that the actual stator frequency of IM is regulated to its reference value, which generates its reference d axis component of stator current, i_{dsim}^* . SG is operated in constant E/f mode through q- axis current control. The reference q axis component of stator current of IM, i_{qsim}^* is calculated using Eqn. (14). The reference (i_{dsim}^* , i_{qsim}^*) and actual d and q axis (i_{dsim} , i_{qsim}) components are shown in Figure 8(k). The d axis current i_{dsim} is inversely proportional to the wind speed v_w , and q axis current i_{qsim} remains constant. Therefore the rms value of stator current of IM (i_{sim}) increases with a decrease in wind speed and vice versa as shown in Figure 8(l). However its value is below its design limit (4 A) and hence the proposed control strategy allows stable operation of IM, leading to smooth variable speed operation of BINSYG.

5. Rapid Control Prototyping (RCP) Verification Results

To verify and validate the performance of the proposed controller, the controller along with the power network is modelled in MATLAB/Simulink and is tested using an OPAL-RT-based real-time simulation platform. The testing is done using two OPAL-RTs, OP 5607 and OP 4520. OP 5607 is used to model the power network while OP 4520 is used to model the controller block. The OPAL-RTs are integrated with two industrial PCs, PC1 and PC2, and they are connected via a dolphin switch. The general specification of the OPAL-RT testbed is specified in Table 5. The steady state and transient results are taken and exhibited in Figures 9 and 10.

5.1. Steady-state results

Steady-state performance analyses are checked by real-time simulations using RT Lab-based OPAL-RT, for two different wind speeds of 7.2 m/s and 12 m/s, and the results are reported in Figure 9. Figure 9(a), (c) shows the R-phase voltage (PWM voltage and its fundamental component) along with the R-phase stator current of SG for steady wind speeds v_w of 7.2 m/s and 12 m/s. The plot reflects that with an increase in wind speed from 7.2 m/s to 12 m/s, the fundamental component and number of levels in the phase voltage of SG increases due

Table 5. General specifications of OPAL-RT testbed

Index	Description
Product used	OP 5607, OP 4520
Operating system	Redhat based Linux real-time operating system
FPGA	OP 5607: Virtex 7 FPGA, OP 4520: Kintex-7 FPGA
Communication	PCI Express links
No of additional I/Os	OP 5607: Up to 96 additional I/Os OP 4520: Up to 128 additional I/Os

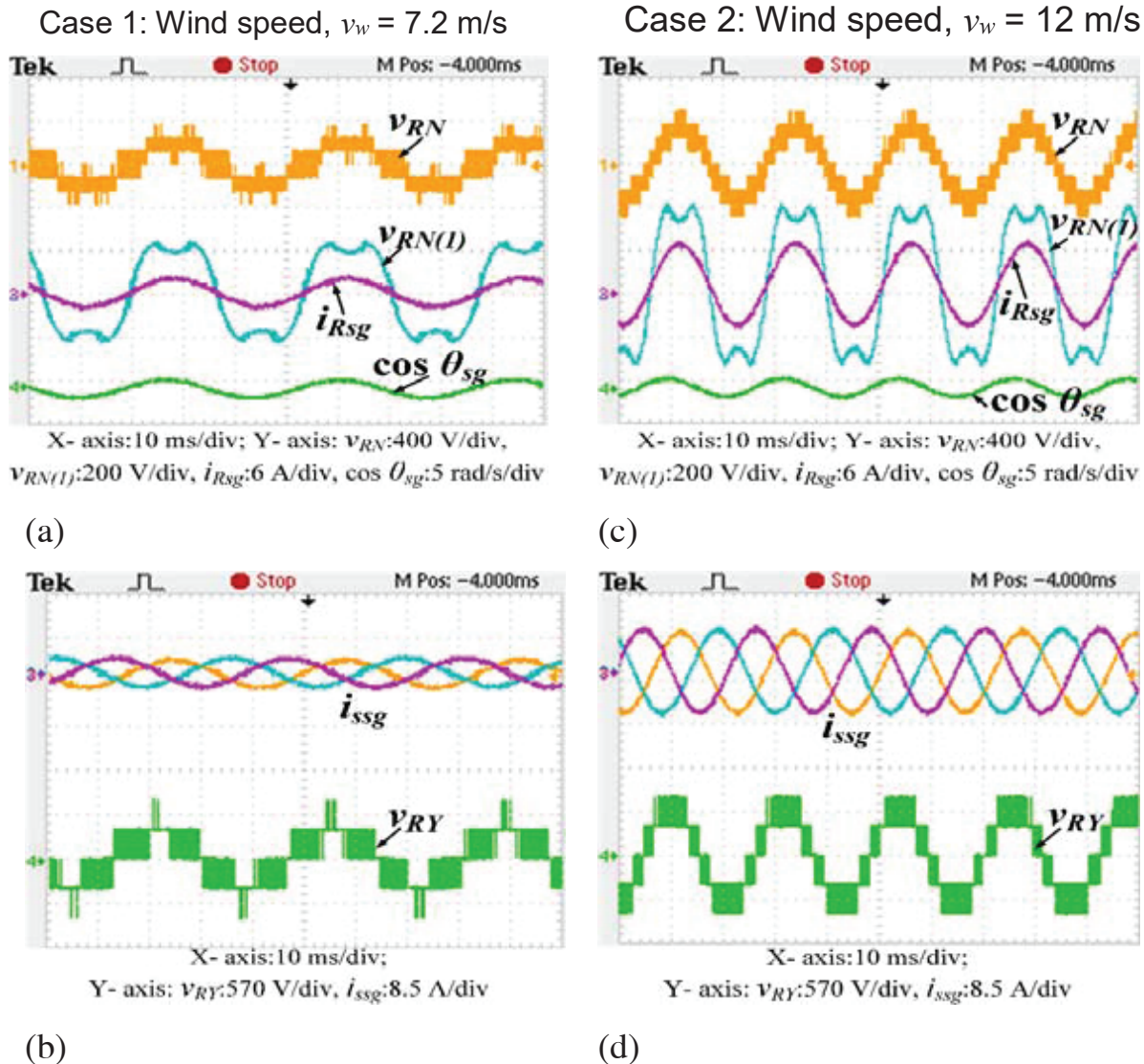


Fig. 9. Steady-state performance of wind turbine connected BINSYG. Case1: when the steady wind speed, v_w is 7.2 m/s. (a) R- Phase Voltage (PWM and fundamental) and R-phase stator current of SG (V_{RN} , $V_{RN(I)}$, i_{Rsg}). (b) three-phase stator current of SG (i_{ssg}), RY-Line voltage of SG (V_{RY}). Case2: when the steady wind speed, v_w is 12 m/s. (c) R- Phase Voltage (PWM and fundamental) and R-phase stator current of SG (V_{RN} , $V_{RN(I)}$, i_{Rsg}). (d) three-phase stator current of SG (i_{ssg}), RY-Line voltage of SG (V_{RY}). BINSYG, brushless induction excited synchronous generator; PWM, pulse width modulated.

to an increase in the modulation index of the rectifier with an increase in wind speed. The modulation of VR allows maintaining upf at stator terminal of SG as shown in the plot. The mechanical position (θ_{sg}) is sensed using the position sensor and its cosine component ($\cos \theta_{sg}$) is obtained and also shown in the figure. This position information is used for voltage vector orientation and modulation of VR. Figure 9(b), (d) shows the line voltage (RY-line) and the three-phase stator currents of SG. The increase in wind speed also increases the power generated by the SG by MPPT control and hence the rms value of stator current of SG increases from 2.2 A to 6.43 A.

5.2. Transient state results

The system experiences a wind speed disturbance where there is a step-change in wind speed (v_w) from 7.2 m/s to 12 m/s at time, $t = 5.0$ s and from 12 m/s to 7.2 m/s at time, $t = 13.5$ s. Real-time simulation results are

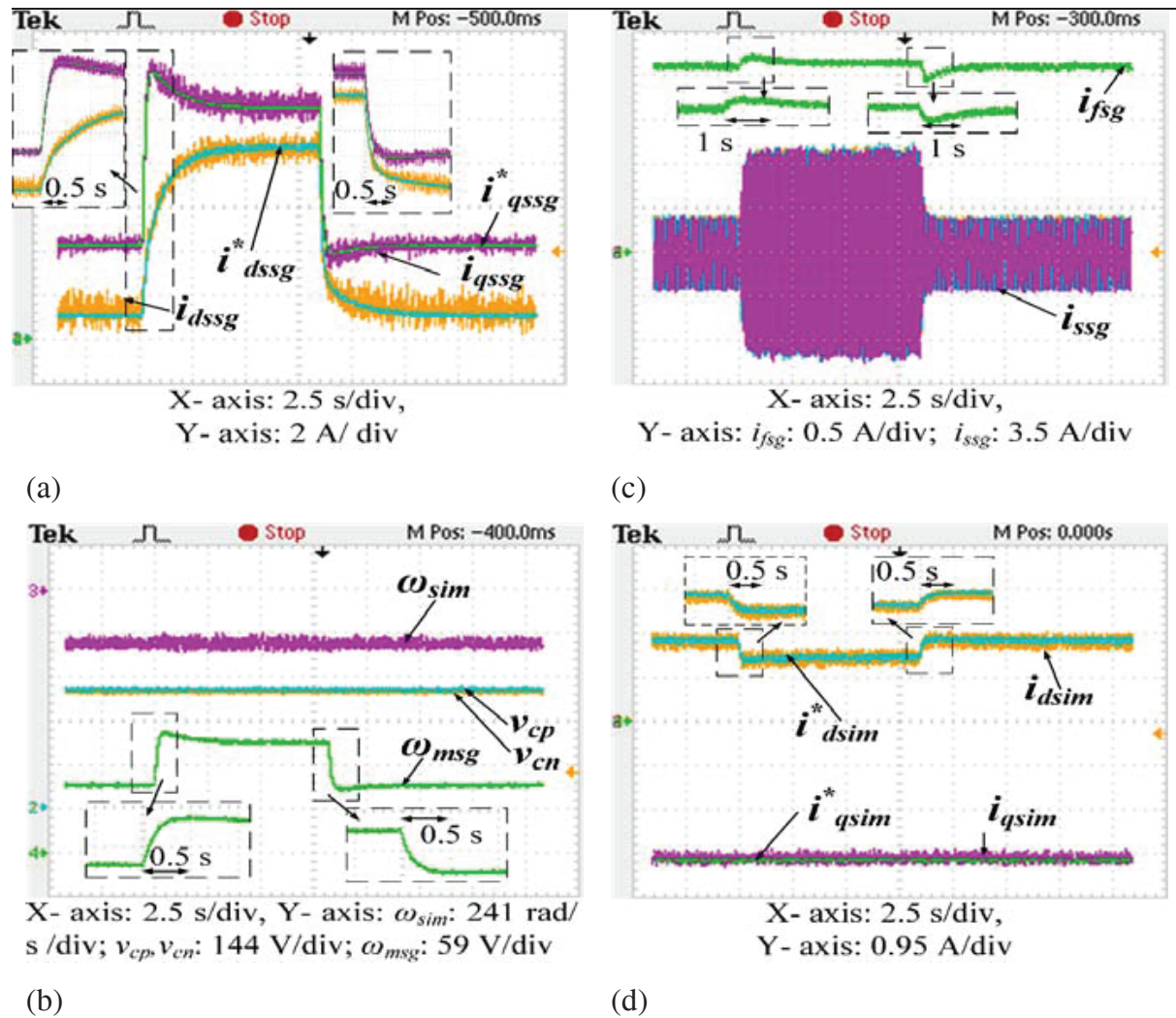


Fig. 10. Steady-state performance of wind turbine connected BINSYG. Case1: when the steady wind speed, v_w is 7.2 m/s. (a) R- Phase Voltage (PWM and fundamental) and R-Phase stator current of SG (V_{RN} , $V_{RN(1)}$, i_{Rsg}). (b) three-phase stator current of SG (i_{ssg}), RY-Line voltage of SG (V_{RY}). Case2: when the steady wind speed, v_w is 12 m/s. (c) R-Phase Voltage (PWM and fundamental) and R-Phase stator current of SG (V_{RN} , $V_{RN(1)}$, i_{Rsg}). (d) three-phase stator current of SG (i_{ssg}), RY-Line voltage of SG (V_{RY}). BINSYG, brushless induction excited synchronous generator; PWM, pulse width modulated.

obtained and presented in Figure 10 to validate the controller performance in transient conditions. The power generated by SG increases with an increase in wind speed following MPPT criterion. The power transferred to the dc grid is regulated by adjusting the reference q axis component of the stator current of SG (i_{qssg}^*). The reference d axis component of stator current of SG (i_{dssg}^*) is tuned to obtain unity pf at the input of VR (SG stator terminal). The actual d and q axis components of stator current of SG (i_{dssg} , i_{qssg}) are sensed. The dynamics of the reference and actual current components are shown in Figure 10(a). It can be observed from the figure that the actual current follows the reference value and this is done by the VR-side current controller. The VR current controller generates the reference d and q axis voltage components which are used for generating modulation signals for VR. Figure 10(b) shows the field current of SG (i_{fsg}) generated by IM-side control and three-phase stator current of SG (i_{ssg}). It is clear from the plot that the field current of SG remains almost constant throughout the period of operation. The dynamics of this current during the wind speed changes are highlighted in the figure. When there is a step-change in wind speed from 7.2 m/s to 12 m/s, the value of i_{fsg} rises by around 0.15 A from its rated value. It again comes back to its rated value of 2.1 A in 1 s. Similarly, when the wind speed

changes from 12 m/s to 7.2 m/s, the value of i_{fsg} falls by around 0.15 A from its rated value and returns to its rated value in 1 s. This figure also shows that the three-phase stator current of SG (i_{ssg}) increases with an increase in wind speed. The top, bottom dc-bus capacitor voltages (v_{cp} , v_{cn}), shaft speed of BINSYG (ω_{msg}) and stator frequency of IM (ω_{sim}) are shown in Figure 10(c). The plot for dc-bus capacitor voltages indicates that the top and bottom capacitor voltages are balanced at 375 V, which is half the dc grid voltage. The capacitor voltages remain balanced even when there is a disturbance in wind speed. The plot for stator frequency of IM (ω_{sim}) indicates that its value is maintained constant at -314 rad/s during the entire period of operation. This shifts the operation of IM to plugging mode that allows stable operation of IM even in a lower range of shaft speeds. The shaft speed changes proportionally to the wind speed. When the wind speed v_w is 12 m/s, the value of ω_{msg} is 157 mech rad/s or 1,500 rpm and when v_w is 7.2 m/s, the value of ω_{msg} is 94.2 mech rad/s or 900 rpm. Thus the proposed IM side controller can allow BINSYG to operate when the shaft speed is lower than 1,000 rpm. The dynamics of the waveform for ω_{msg} are also highlighted in the figure. The 2L VSI control for governing the IM stator current magnitude and frequency is done by d and q axis current control. The reference d axis current is set through regulation of stator frequency of IM to its reference value. This reference value is chosen such that IM operates in plugging mode. The reference q axis current is constant and calculated to allow the development of the rated field current. The actual stator currents of IM are sensed and converter to dq axis components and are presented in Figure 10(d). The figure shows that the actual dq axis current components are regulated to their reference values.

Therefore, steady state and transient MATLAB/Simulink and real-time simulations validate the effectiveness of the controller during steady and step change in wind speed. The generator BINSYG is able to feed maximum power to the dc grid according to the wind speed. The proposed IM side VSI controller is able to generate the required field current of SG while keeping the constant magnitude of stator current of IM. This controller is also able to operate the IM when the shaft speed is lower than 1,000 rpm. As a result, BINSYG is able to generate and transfer power for varying wind speeds.

6. Conclusion

The performance of variable speed wind turbine connected BINSYG feeding power to a stiff dc grid is reported in this paper. BINSYG is connected to a 2L VSI on the stator side of IM that is used to develop and control the excitation of SG via control of the stator current of IM. On the stator side of SG, it is tied up to a dc grid via a 3L VR, which controls the magnitude and quality of power flow to the dc grid. A new controller is developed for 2L VSI to control the field current of SG through regulating voltage and current fed to IM. The proposed controller forces the operation of IM to plugging mode by setting its stator frequency at -314 elec rad/s. The field current of SG is developed and guided by setting reference q-axis current of IM, according to the rated field current requirement. The advantage of the controller is that it can operate IM in stable mode at shaft speeds below 1,000 rpm. Hence the proposed control strategy can operate the variable speed wind turbine connected BINSYG smoothly at MPP condition from cut-in wind speed to rated wind speed. A VR controller is developed to ensure upf at SG stator terminals, improved power quality of stator current of SG, MPP operation of SG and also balancing of top and bottom dc-bus capacitors. A 5.5 kVA, 415 V BINSYG with 3L VR connected to SG stator and 2L VSI connected to IM stator is modelled using MATLAB/Simulink. The effectiveness of the proposed system and controller is first checked with steady wind speeds and then with a step-change in wind speed. The simulation results show the effectiveness and stable operation of BINSYG under both steady and transient conditions. These are verified from RCP results obtained using the OPAL-RT testbed. Thus the proposed brushless and permanent magnetless machine along with the 3L VR is very promising for wind electric power conversion system feeding power to dc grids.

Author Contributions

HB – Research concept and design, Collection and/or assembly of data, Data analysis and interpretation, writing the article. DM – Research concept and design, Critical revision of the article. CC – Research concept and design, Critical revision of the article, Final approval of the article.

References

- Bhattacharjee, H., Mukherjee, D., Vuyyuru, U. and Chakraborty, C. (2021). Brushless Synchronous Generator-Unidirectional Rectifier for Offshore Wind Energy Conversion System. *IEEE Transactions on Energy Conversion*. Available at: <https://ieeexplore.ieee.org/document/9629266>
- Bhattacharjee, H., Rao, Y. T. and Chakraborty, C. (2020). Brushless and Magnetless Synchronous Generator for Standalone DC Load with Vienna Rectifier. *IEEE 29th International Symposium on Industrial Electronics (ISIE)*, Delft, Netherlands, pp. 83–88.
- Bose, B. K. (2002). *Modern Power Electronics and AC Drives*. New Jersey, United States: Prentice Hall PTR.
- Chakraborty, C. and Rao, Y. T. (2019). Performance of Brushless Induction Excited Synchronous Generator. *IEEE Journal of Emerging and Selected Topics in Power Electronics*, 7(4), pp. 2571–2582.
- Flores-Bahamonde, F., Valderrama-Blavi, H., Martínez-Salamero, L., Maixé-Altés, J. and García, G. (2014). Control of a Three-Phase AC/DC VIENNA Converter Based on the Sliding Mode Loss-free Resistor Approach. *IET Power Electronics*, 7(5), pp. 1073–1082.
- Gajewski, P., and Pieńkowski, K. (2016). The Performance of Direct-Driven Variable Speed Wind Turbine With Pmsg And Converter Systems. *Power Electronics and Drives*, 1, pp. 79–89.
- Gil, M. D. P., Domínguez-García, J. L., Díaz-González, F., Aragüés-Peñalba, M., Gomis-Bellmunt, O. (2015). Feasibility Analysis of Offshore Wind Power Plants With DC Collection Grid. *Renewable Energy*, 78, pp. 467–477.
- Global Wind Report 2021. (2021). *GWEC*. Available at: <https://gwec.net/global-wind-report-2021/> Accessed: December 2021.
- Heier, S. (2014). *Grid Integration of Wind Energy: Onshore and Offshore Conversion Systems*, 3rd ed. New York: Wiley.
- Iwański, G., and Łuszczczyk, T. (2017). Control of Doubly Fed Induction Generator at Grid Voltage Imbalance. *Power Electronics and Drives*, 2, pp. 31–48.
- Kumari, S., Kushwaha, V. and Gupta, T. N. (2018). A Maximum Power Point Tracking for a PMSG Based Variable Speed Wind Energy Conversion System. 2018 International Conference on Power Energy, Environment and Intelligent Control (PEEIC), Greater Noida, India, 2018, pp. 789–794.
- Lee, J. and Lee, K. (2015). Open-Switch Fault Tolerance Control for a Three-Level NPC/T-Type Rectifier in Wind Turbine Systems. *IEEE Transactions on Industrial Electronics*, 62(2), pp. 1012–1021.
- Lee, J. and Lee, K. (2017). Predictive Control of Vienna Rectifiers for PMSG Systems. *IEEE Transactions on Industrial Electronics*, 64(4), pp. 2580–2591.
- Liu, Y., Pehrman, D., Lykartsis, O., Tang, J. and Liu, T. (2016). High Frequency Exciter of Electrically Excited Synchronous Motors for Vehicle Applications. *2016 XXII International Conference on Electrical Machines (ICEM)*, pp. 378–383.
- Luqman, M., Yao, G., Zhou, L. and Lamichhane, A. (2019). Analysis of Variable Speed Wind Energy Conversion System with PMSG and Vienna Rectifier. *IEEE 14th Conference on Industrial Electronics and Applications (ICIEA)*, pp. 1296–1301.
- Maswood, A. I., Al-Ammar, E. and Liu, F. (2011). Average and Hysteresis Current-Controlled Three-Phase Three-Level Unity Power Factor Rectifier Operation and Performance. *IET Power Electronics*, 4(7), pp. 752–758.
- Minibock, J. and Kolar, J. W. (2005). Novel Concept for Mains Voltage Proportional Input Current Shaping of a VIENNA Rectifier Eliminating Controller Multipliers. In: *IEEE Transactions on Industrial Electronics*, 52(1), pp. 162–170.
- Moallem, M., Mirzaeian, B., Mohammed, O. A., and Lucas, C. (2001). Multi-Objective Genetic-Fuzzy Optimal Design of PI Controller in the Indirect Field Oriented Control of an Induction Motor. *IEEE Transactions on Magnetics*, 37(5), pp. 3608–3612s.
- Mukherjee, D. and Kastha, D. (2015). Voltage Sensorless Control of the Three-Level Three-Switch Vienna Rectifier with Programmable Input Power Factor. *IET Power Electronics*, 8(8), pp. 1349–1357.
- Patin, N., Vido, L., Monmasson, E., Louis, J., Gabsi, M. and Lecrivain, M. (2008). Control of a Hybrid Excitation Synchronous Generator for Aircraft Applications. *IEEE Transactions on Industrial Electronics*, 55(10), pp. 3772–3783.
- Pavel, C. C., Lacal-Aránategui, R., Marmier, A., Schüler, D., Tzimas, E., Buchert, M., Jenseit, W. and Blagoeva, D. (2017). Substitution Strategies for Reducing the Use of Rare Earths in Wind Turbines. *Resources Policy*, 52, pp. 349–357.
- Prajapat, G. P., Senroy, N. and Kar, I. N. (2021). Estimation Based Enhanced Maximum Energy Extraction Scheme for DFIG-Wind Turbine Systems. *Sustainable Energy, Grids and Networks*, 26, p. 100419.

- Rahimi, M. (2017). Modeling, Control and Stability Analysis of Grid Connected PMSG Based Wind Turbine Assisted with Diode Rectifier and Boost Converter. *International Journal of Electrical Power & Energy Systems*, 93, pp. 84–96.
- Rajaei, A. H., Mohamadian, M., Dehghan, S. M. and Yazdian, A. (2011). PMSG-based Variable Speed Wind Energy Conversion System Using Vienna Rectifier. *European Transactions on Electrical Power*, 21, pp. 954–972.
- Rao, Y. T., Chakraborty, C. and Sengupta, S. (2021). Performance and Stability of Brushless Induction Excited Synchronous Generator Operating in Self-Excited Mode for Wind Energy Conversion System. *IEEE Transactions on Energy Conversion*, 36(2), pp. 919–929.
- Reddy, D. and Ramasamy, S. (2018). Design of RBFN Controller Based Boost Type Vienna Rectifier for Grid-Tied Wind Energy Conversion System. *IEEE Access*, 6, pp. 3167–3175.
- Sabrina, U., Schullerus, G. and Soenmez, E. (2021). Active Damping in Series Connected Power Modules with Continuous Output Voltage. *Power Electronics and Drives*, 6(41), pp. 314–335.
- Shipurkar, U., Strous, T. D., Polinder, H., Ferreira, J. A. and Veltman, A. (2017). Achieving Sensorless Control for the Brushless Doubly Fed Induction Machine. *IEEE Transactions on Energy Conversion*, 32(4), pp. 1611–1619.
- Szulawski, P. and Koczara, W. (2016). Synchrogenverter-Parallel Connection of Synchronous Generator and Power Converter with Energy Storage. *Power Electronics and Drives*, 1, pp. 69–78.
- Xu, J. and Xie, S. (2018). LCL-Resonance Damping Strategies for Grid-Connected Inverters with LCL Filters: A Comprehensive Review. *Journal of Modern Power Systems and Clean Energy*, 6, pp. 292–305.
- Yang, G. and Zhu, Y. (2010). Application of a Matrix Converter for PMSG Wind Turbine Generation System. *The 2nd International Symposium on Power Electronics for Distributed Generation Systems*, Hefei, China, pp. 185–189.
- Yaramasu, V., Wu, B., Sen, P. C., Kouro, S., and Narimani, M. (2015). High-Power Wind Energy Conversion Systems: State-of-the-Art and Emerging Technologies. *Proceedings of the IEEE*, 103(5), pp. 740–788.